Proceedings of ASME Turbo Expo 2011
GT2011
June 6-10, 2011, Vancouver, British Columbia, Canada

GT2011-45686

THERMAL MODELING OF A SOLAR STEAM TURBINE WITH A FOCUS ON START-UP TIME REDUCTION

James Spelling
Royal Institute of Technology
Heat and Power Technology
100 44 Stockholm, Sweden

Markus Jöcker
Siemens Industrial
Turbomachinery AB
612 83 Finspång, Sweden

Andrew Martin
Royal Institute of Technology
Heat and Power Technology
100 44 Stockholm, Sweden

ABSTRACT

Steam turbines in solar thermal power plants experience a much greater number of starts than those operating in base-load plants. In order to preserve the lifetime of the turbine whilst still allowing fast starts, it is of great interest to find ways to maintain the turbine temperature during idle periods. A dynamic model of a solar steam turbine has been elaborated, simulating both the heat conduction within the body and the heat exchange with the gland steam, main steam and the environment, allowing prediction of the temperatures within the turbine during off-design operation and standby. The model has been validated against 96h of measured data from the Andasol 1 power plant, giving an average error of 1.2% for key temperature measurements. The validated model was then used to evaluate a number of modifications that can be made to maintain the turbine temperature during idle periods. Heat blankets were shown to be the most effective measure for keeping the turbine casing warm, whereas increasing the gland steam temperature was most effective in maintaining the temperature of the rotor. By applying a combination of these measures the dispatchability of the turbine can be improved significantly: electrical output can be increased by up to 9.5% after a long cool-down and up to 9.8% after a short cool-down.

1 INTRODUCTION

Steam turbine operation in solar thermal power plants is very different than in traditional base-load power plants. As a result of the variable nature of the solar supply and the daily operating cycle of solar power plants, the number of turbine starts per year for solar steam turbines is an order of magnitude higher than for base-load turbines. This requires turbine component optimization to avoid excessive thermal stresses and low cycle fatigue in the casing and rotor of the turbine during start-up, shut down and load variations [1]. Due to the uncontrollable nature of the solar supply, it is also desirable that the turbine be able to start as quickly as possible, in order for the power plant to be available to harness the Sun's energy whenever it is available. In order to avoid excessive thermal stresses within the turbines during start-up, and thus preserve the lifetime of the units, the manufacturer specifies start-up curves which limit the speed at which the turbines can reach full load, based on the lowest metal temperature measured before start-up begins, as shown in Figure 1.

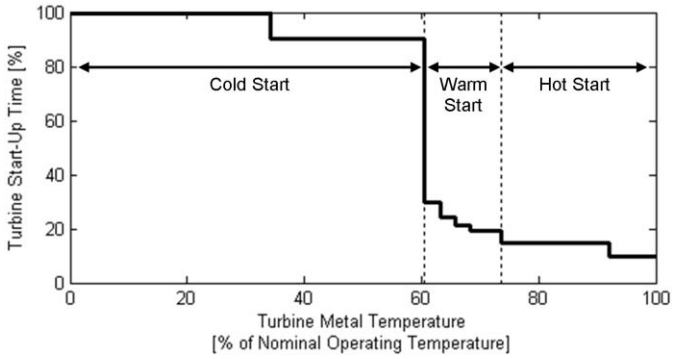

Figure 1: Turbine start-up time as a function of the minimum temperature measured in the unit before start-up.

Previous studies ([2], [3]) have focused on the reduction of rapid temperature and pressure transients in the solar steam supply during operation in order to avoid excessive thermal stresses and the corresponding lifetime reduction. Other works have studied means of changing operating procedures to achieve faster start-up times [4]. Prior simulation work using Modelica [5] has analyzed the turbine performance during solar transients, though only a simplified lumped-mass model was used for the evaluation of wall temperatures and thermal gradients within the turbine units

All these studies overlook a potential area for operational improvement, namely that the limiting factor in achieving faster

starts without harming the turbine is the cooling down of the metal during idle periods. If the steam turbine can be kept hot during idle periods, the duration of the next start-up can be reduced without impacting negatively on the lifetime.

In this work, a detailed transient thermal model of a solar steam turbine is presented and validated, in order to obtain accurate information about the metal temperatures during off-design operation and stand-by. Methods are then presented for maintaining the turbine temperatures during stand-by in order to safely benefit from the increased speeds of warm and hot start-ups, thus improving the dispatchability of the turbines.

NOMENCLATURE

Symbols

E	Mechanical Power	[W]
G	Mass Flux	[kg/m^{2}s]
h	Specific Enthalpy	[J/kg]
k	Thermal Conductivity	[W/mK]
M	Mass Flow Rate	[kg/s]
n	Number of Timesteps	[-]
N	Rotational Speed	[rpm]
T	Temperature	[K]
P	Pressure	[Pa]
Q	Thermal Power	[W]
Y	Ellipse Constant	[-]
α	Heat Transfer Coefficient	[W/m^{2}K]
ε	Heat Transfer Effectiveness	[-]
Π	Pressure Ratio	[-]
ς	Void Fraction	[-]

Subscripts

a	Axial
adb	Adiabatic
cond	Condenser
ext	Extraction Point
gst	Gland Steam
HP	High Pressure
HPT	High Pressure Turbine
LP	Low Pressure
LPT	Low Pressure Turbine
m	Metal
o	Nominal Point
r	Radial
s	Isentropic
st	Steam

2 SOLAR STEAM TURBINE

The turbine under study is the SST-700RH Solar, a 50 MW reheat system comprised of high-pressure and low-pressure turbine units, with steam extraction occurring from both units. This turbine is employed in numerous solar thermal power plants worldwide. For the purpose of this work, the standard control instrumentation of the turbine was supplemented with additional temperature measurements points on the casings of the two units, as shown in Figure 2.

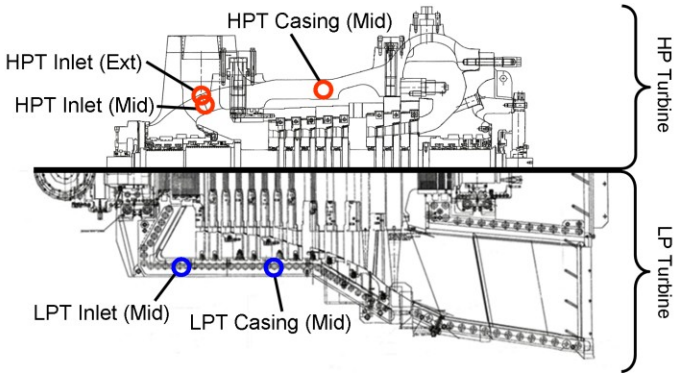

Figure 2: High- and low-pressure units of the SST-700RH, including the location of the casing temperature measurement points (not to scale).

3 DYNAMIC STEAM TURBINE MODEL

The steam turbine model has been developed using MATLAB classes in order to allow integration with an existing in-house tool [6] for the dynamic simulation and optimization of solar thermal systems. The key purpose of the model will be the prediction of the metal temperatures within the turbine both during operation and stand-by. To achieve this, the steam turbine is simulated using a coupled model, composed of three interconnected parts:

1. A finite-volume heat conduction model to evaluate the casing and rotor metal temperatures.
2. A thermodynamic model to determine the steam expansion temperatures during operation, along with the corresponding heat transfer coefficients.
3. A separate gland steam network model to calculate the temperatures and heat fluxes in the labyrinth joints.

In preparation for the elaboration of the simulation model, it is necessary to define the boundaries of the system under study. Due to the availability of measured input data for the turbine in question, it was not necessary to simulate the entire power plant in order to analyze the dynamic behavior of the turbine unit.

3.1 Transient Heat Conduction Model

The core of the model comprises a finite volume model for the heat conduction within the solid turbine components. The true geometry of the solar steam turbine forms a complex 3D entity which it is beyond the scope of this study to model in full detail. In order to facilitate the modeling, a 2D axisymmetric model has been used for each turbine unit, which is sufficient to predict the required temperatures with an acceptable accuracy, as is confirmed by the validation results presented in §4.3.

Within the turbine, the blade disks form a region of very convoluted geometry, the full detail of which is not modeled in this work. Instead, the blade disks are considered to be a region of anisotropic heat conduction, with preferential conduction in the radial direction. The axial and radial heat conduction coefficients, k_a and k_r respectively, can be determined using equations (1) and (2), where ς is the void fraction in the disk

region and k_{st} and k_m are the steam and metal thermal conductivities respectively. This approach assumes Couette flow [7] in the disk regions with negligible viscous heating.

$$\frac{1}{k_a} = \frac{\varsigma}{k_{st}} + \frac{1-\varsigma}{k_m} \quad (1)$$

$$k_r = \varsigma \cdot k_{st} + (1-\varsigma) \cdot k_m \quad (2)$$

Outside the blade disk regions, the standard isotropic heat conduction equations are applied. The breakdown of the conduction domains within the steam turbine units is shown in Figure 3. The rotor and casing blocks are considered as isotropic solid metal, whereas the two blade disk regions apply the anisotropy specified in equations (1) and (2).

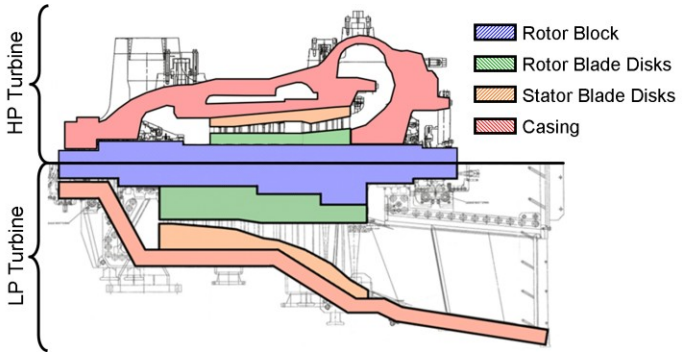

Figure 3: High- and low-pressure units of the SST-700RH, showing the geometry blocks in which the different heat conduction equations apply.

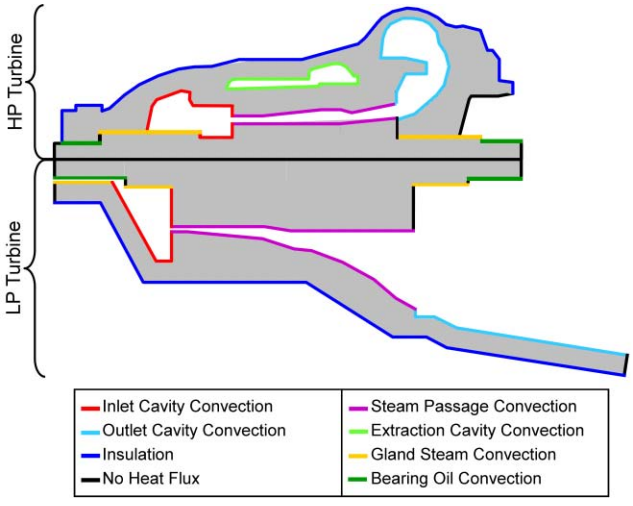

Figure 4: High- and low-pressure sections of the finite-volume model, showing the different boundary conditions.

The transient heat conduction equations are solved using a node-centered finite-volume technique [8], with a first-order implicit Euler scheme [9] applied to the temporal derivatives.

The boundary conditions applied to the model are shown in Figure 4. The insulation boundary takes into account heat losses by conduction through an external layer of insulation followed by natural convection to the surroundings. Ambient temperatures for the heat losses are taken from on-site measurements. The heat fluxes at the convective boundaries are determined using the other subsections of the coupled model. The steam expansion model calculates steam temperatures within the flow passage, along with the mass flow rate which is necessary to fix the heat transfer coefficients. Similarly, the gland steam network model supplies the temperatures and heat exchange within the labyrinth joints.

3.2 Steam Expansion Model

To be able to calculate the heat transfer within the flow passages, it is necessary to resolve the steam temperature and pressure profiles within the blade passage of each turbine unit. In order to be able to achieve this by applying Stodola's ellipse law [10], the turbine is divided into a number of segments between the steam extraction points, as shown in Figure 5, within which ellipse constants Y can be calculated. The nominal isentropic efficiencies η_s are specified by the manufacturer for each segment.

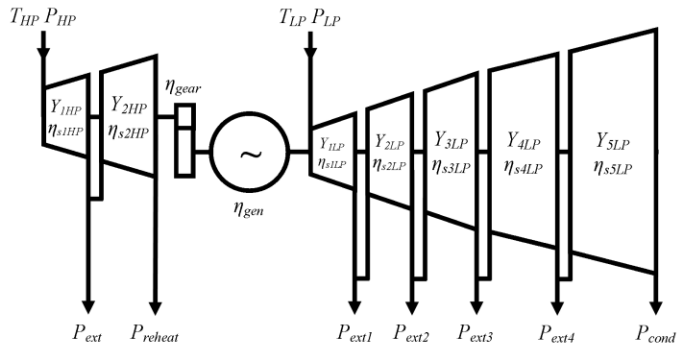

Figure 5: Input and boundaries of the steam turbine model, including segments for Stodola modeling.

The Stodola approach applies in the case of an adiabatic expansion; however, in the case presented here, heat transfer will occur between the steam and the blades. In order to take into account this effect, the total heat transferred over each segment is calculated and considered to be exchanged with the steam flow at constant pressure after the expansion. This approximation can be represented as shown in Figure 6.

The true expansion from h_{in} to h_{out} is broken down into the adiabatic expansion h_{in} - h_{adb}, during which power E is extracted from the flow, followed by the isobaric heat transfer from h_{adb} to h_{out}. Thus, the true enthalpy at the exit of the segment is given by (3), where Q is the total heat transferred between the turbine and the steam within the segment and M the mass flow.

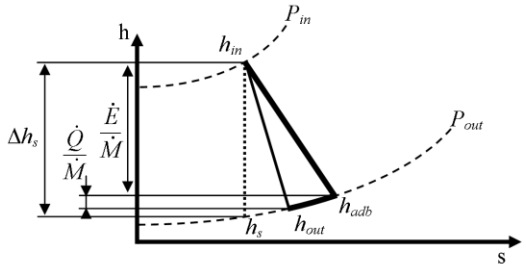

Figure 6: Steam expansion h-s diagram, showing the different terms involved in the temperature calculations.

$$h_{out} = h_{in} - \frac{\dot{E}}{\dot{M}} - \frac{\dot{Q}}{\dot{M}} \tag{3}$$

The calculation of h_{adb} requires knowledge of the isentropic efficiency η_s of the segment. Based on the nominal value η_{so} provided by the manufacturer, the off-design efficiencies can be calculated using a correlation (4) proposed by Ray [11], where N is the rotational speed of the unit and Δh_s the isentropic enthalpy variation.

$$\eta_s = \eta_{so} - 2\left(\frac{N}{N_o}\sqrt{\frac{\Delta h_{so}}{\Delta h_s}} - 1\right)^2 \tag{4}$$

The heat transfer coefficients within the flow passages are calculated based on nominal values specified by the turbine manufacturer, shown in Figure 7.

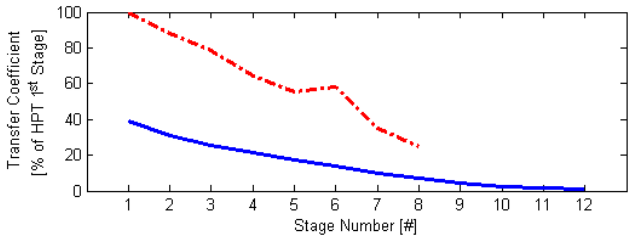

Figure 7: Flow passage heat transfer coefficients.

The off-design values are calculated using a correlation (5) provided by the turbine manufacturer, where T_{in} is the inlet temperature, P_{in} and P_{out} are the inlet and outlet pressures respectively and $\Pi = P_{out}/P_{in}$ is the pressure ratio across the section. The subscript o refers to the design values.

$$\frac{\alpha}{\alpha_o} = \left(\frac{\dot{M}}{\dot{M}_o}\right)^{0.8} = \left(\frac{P^{in}}{P_o^{in}}\sqrt{\frac{T^{in}}{T_o^{in}}\frac{\left(1-\Pi^2\right)}{\left(1-\Pi_o^2\right)}}\right)^{0.8} \tag{5}$$

3.3 Gland Steam Network Model

In order to prevent the infiltration of air within the turbines, the labyrinth joints must be provided with an external supply of steam (known as gland steam) during idle periods and low-load operation. This is shown schematically in Figure 8. It is also necessary to provide external gland steam to the low-pressure-side labyrinth of the low-pressure turbine even during full-load operation, due to the vacuum conditions found within the condenser.

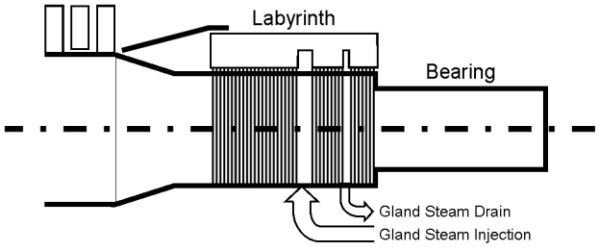

Figure 8: Steam turbine rotor showing gland steam injection

The boundary heat flux q within the joints is modeled (6) assuming a heat exchange effectiveness ε [7] for the heat transfer between the gland steam temperature T_{gst} and the surface metal temperature T_m, where G is the mass flux through the labyrinth and c_p the average heat capacity of the steam between the two temperatures.

$$q = \varepsilon G c_p \left(T_{gst} - T_m\right) \tag{6}$$

The external gland steam network provides two levels of steam for injection into the labyrinths on either the high-pressure or low-pressure side, with potentially a different temperature for each. When the turbine is idle, the gland steam temperature is fixed entirely by the external supply. During part-load operation, the temperature of the gland steam is determined by the mixing of the externally supplied steam and the internal steam leakage from the inlet and exhaust cavities. The fraction of the gland steam delivered by the external supply is shown in Figure 9 for different turbine loads. Above 60% load, the gland steam supply is entirely self-sustaining.

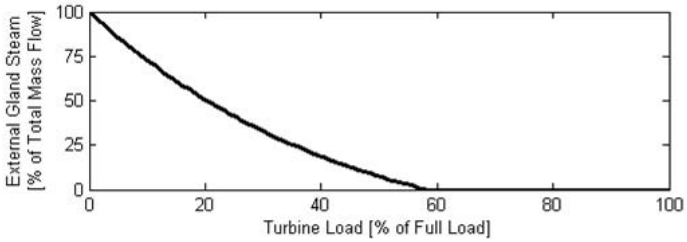

Figure 9: Fraction of gland steam supplied by the external steam source.

4 MODEL VALIDATION

In order to validate the predictions made by the dynamic steam turbine model, 96h of operation data for the steam turbines of the Andasol 1 power plant were made available. A number of supplementary temperature measurements were taken for the turbines, as was shown in Figure 2.

4.1 Validation Data

The input data used for the validation of the steam turbine models is shown in Figure 10. The four days of data feature three relatively standard operation days (21st, 23rd and 24th October), which involve a number of turbine starts and stops due to insufficient insolation. On the remaining day (22nd October), no operation of the plant was possible due to poor meteorological conditions, resulting in a shut-down of more than 24 hours of the steam turbine units. The wide variety of operating conditions experienced by the turbines during the measurement period allows the dynamics of the model to be validated across a nearly complete range of situations likely to be encountered, namely start-up, short cool-down (<10h), long cool-down (>24h) and load variation.

The measured turbine casing temperature values are shown in Figure 11. It is against these values that the output of the simulation model will be validated.

4.2 Model Correction using a Genetic Algorithm

Initial validation results using the heat transfer coefficients provided by the manufacturer of the turbines gave an average relative error of 3.8%, however the prediction of the cool-down temperatures showed a maximum error of 12.1% which was judged unacceptable.

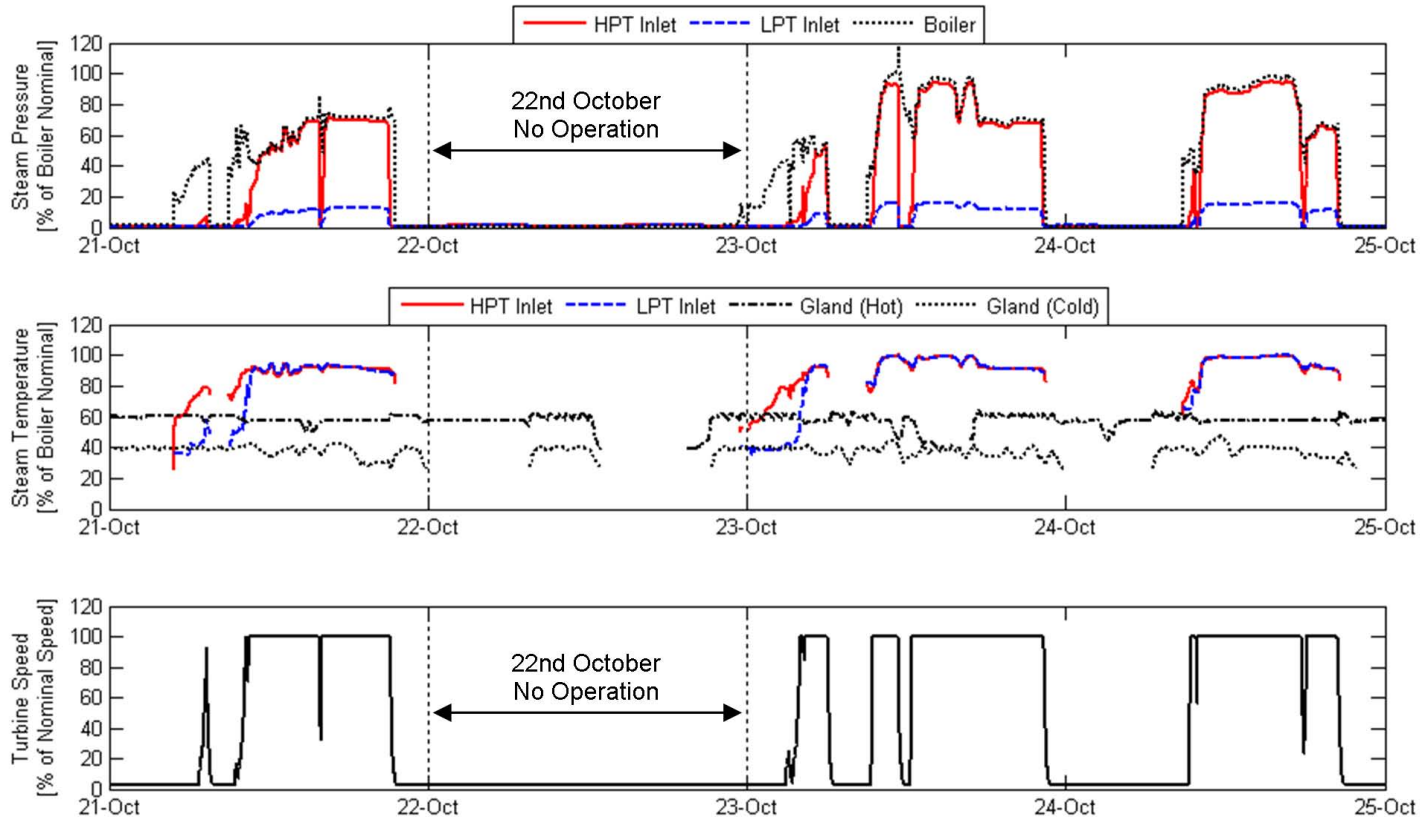

Figure 10: Validation input data for the steam turbine models. Steam temperature and pressure given as percentage of nominal boiler values. Due to insufficient insolation, the plant was not operated on the 22nd October.

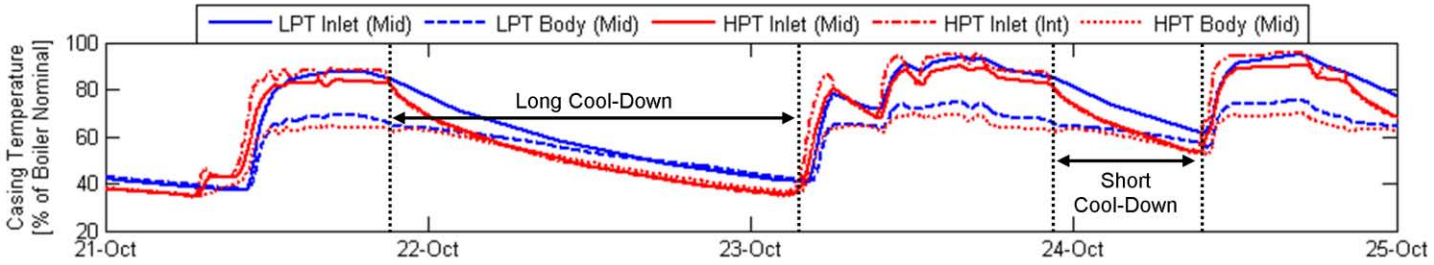

Figure 11: Validation output data for the steam turbine models. Temperature given as percentage of nominal boiler value.

This error resulted from a number of geometrical parameters that were not able to be obtained with a sufficient level of detail, notably for the heat transfer within the flow passages and labyrinth joints. In order to rectify this situation whilst still remaining as faithful as possible to the specifications provided by the manufacturer, a number of correction factors (shown in Table 1) were applied to the heat transfer values and the multi-objective genetic optimization algorithm QMOO [12] used to select appropriate values. By using multi-objective optimization, it was possible to simultaneously aim for a minimum error in the predictions of the model as well as minimum magnitude of the correction factors applied to the model.

#	Factor	Affected Heat Transfer Terms
1	*fcond*	Flow Passage Conduction
2	*flabyrinth*	Gland Steam Effectiveness
3	*fbear*	Bearing Oil Convection
4	*fLPst*	LP Turbine Flow Passage
5	*fLPcav*	LP Turbine Inlet Cavity LP Turbine Exhaust
6	*fLPext*	LP Turbine Heat Losses
7	*fHPst*	HP Turbine Flow Passage
8	*fHPcav*	HP Turbine Inlet Cavity HP Turbine Exhaust
9	*fHPextr*	HP Turbine Extraction Cavity
10	*fHPext*	HP Turbine Heat Losses

Table 1: Steam turbine heat transfer coefficient correction factors. All values limited between −1 and +1.

Based on the value selected for the correction factor f_{corr}, the new nominal value of the heat transfer coefficient is calculated using (7).

$$\alpha_{corr} = \alpha_o \cdot 10^{f_{corr}} \tag{7}$$

The two objective functions defined for the optimization are the minimization of the average magnitude of the relative error ε_{rel} (8) and the minimization of the absolute magnitude M_{corr} of the correction (9). In these equations n is the total number of measurement-points / simulation-timesteps, Δt the measurement / simulation timestep and T_{sim} and T_{mes} are respectively the simulated and measured values of the temperature at each timestep.

The minimization of the two objective functions (8) and (9) will be conflicting, as the average absolute error will decrease as the magnitude of the correction increases. A multi-objective optimization algorithm is therefore well adapted to study a problem of this nature [13]. The different correction factors shown in Table 1 are the decision variables made available to the optimization algorithm.

$$\bar{\varepsilon}_{rel} = \frac{1}{n}\sum_{i=1}^{n}\left|\frac{T_{sim}(i\Delta t) - T_{mes}(i\Delta t)}{T_{mes}(i\Delta t)}\right| \tag{8}$$

$$M_{corr} = \sum_{j=1}^{10}\left|f_{corr}\right| \tag{9}$$

The algorithm population after 600 model evaluations is shown in Figure 12, along with the position of the Pareto-optimal front [12]. A point can be defined as being Pareto-optimal if there exists no other point within the decision space that is better in *all* objectives. By choosing a solution on the Pareto front, naïve solutions are avoided and, of all the feasible solutions, only those that satisfy as best as possible *all* objectives are considered.

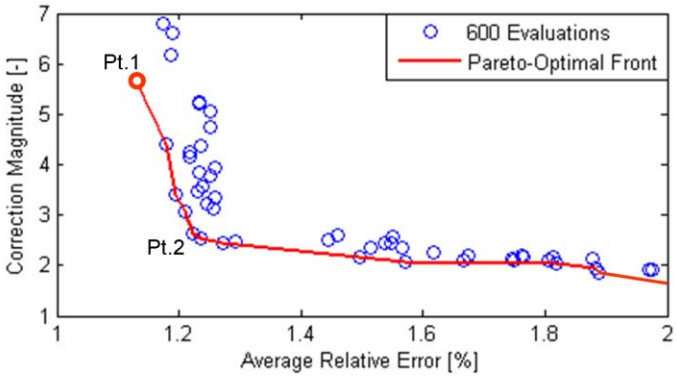

Figure 12: Evolutionary algorithm population after 600 evaluations. Position of the Pareto-optimal front shown in red.

Point 1 in Figure 12 is the Pareto-optimal point with the lowest relative error but it displays a very high correction magnitude. For this study, the correction factor values from Point 2 are chosen. This Pareto-optimal point maintains a low relative error (at 1.2% average error) but sits before the inflection point on the Pareto curve, giving a much lower correction magnitude and thus more confidence in the model.

4.3 Validation Results

The evolution of the relative error between the temperature measurements and the simulated values is shown in Figure 13, along with a more direct comparison between the measured and simulated casing temperatures. It can be seen that the largest values of the relative error occur during the start-up phases, where the most rapid changes in operating condition occur. The peak relative error during these phases is 7.5%, during the cool-down phases it is considerably lower. The transient behavior of the temperatures is thus well captured.

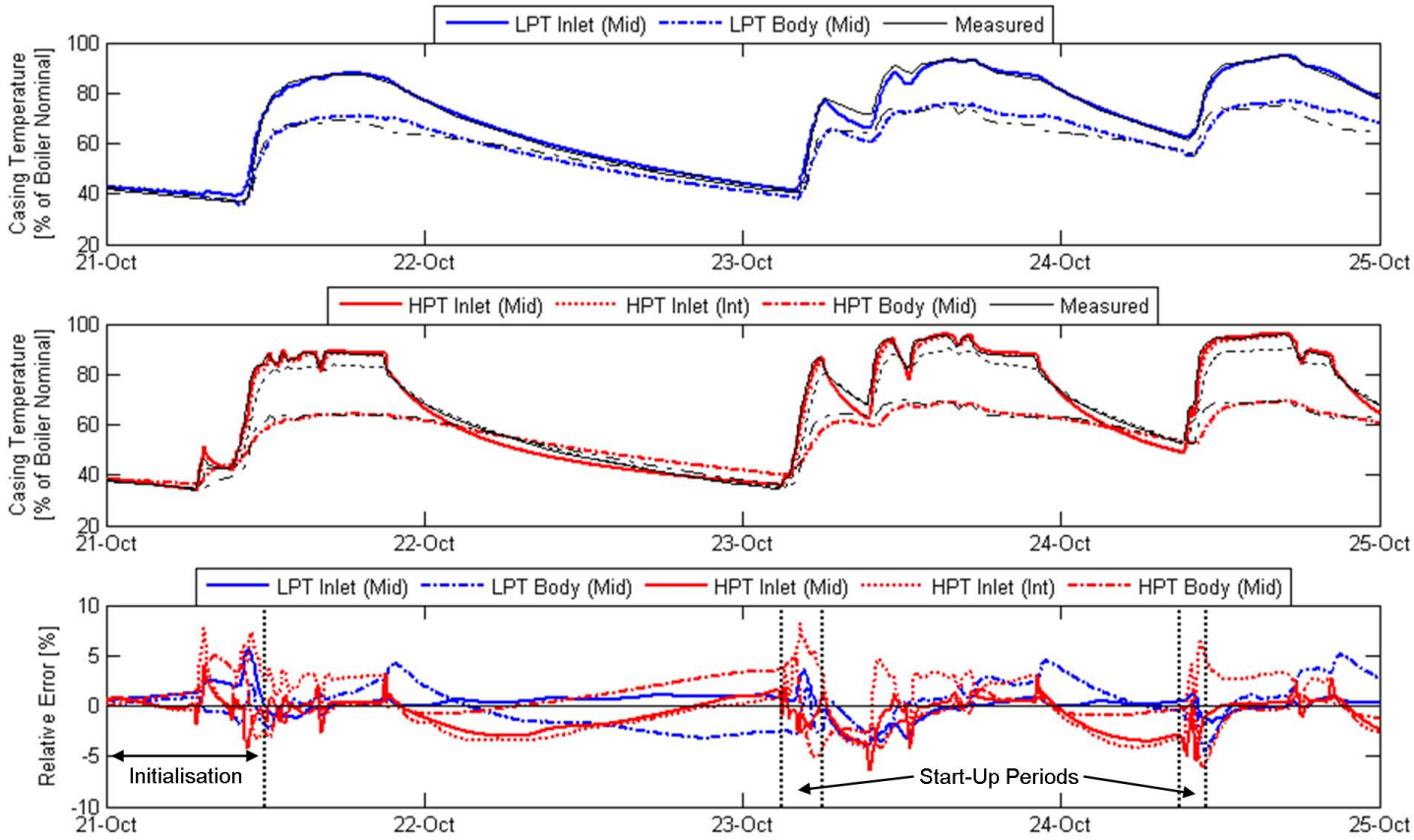

Figure 13: Comparison between simulated values and measured data for the optimized steam turbine models. Thick colored lines show simulated values, thin black lines show measurements. Temperatures given as percentage of nominal boiler temperature.

It should be pointed out here however that a degree of uncertainty persists regarding the rotor temperatures, due to the lack of any validation data for the turbine rotors and the difficulty of evaluating analytically the rate of heat transfer across the blade passage when the turbine is idle. Access to reliable temperature measurements for the rotor would greatly improve the quality of these predictions.

4.4 Sensitivity Analysis

As a number of correction factors were applied in order to obtain these validation results, it is also necessary to examine the sensitivity of the turbine model to the corrections applied. The results of this analysis is presented in Figure 14 which shows the values of the correction factors used, alongside their maximum influence on the measured temperatures within a ±25% range around the selected value. The correction factor numbers correspond to those in Table 1.

The first two influence bars in Figure 14 show the maximum change in the measured casing and rotor temperatures during the whole simulation period. The second two bars give the maximum change in casing and rotor temperature measured just before start-up. It is this second set of temperatures that are crucial for the determination of the start-up speed. With a ±25% variation in the correction values, it can be seen that the maximum influence on the simulated temperatures is below 3%, and the influence on the key pre-start-up temperatures is below 2%. Globally, it can be seen that the pre-start-up temperatures are relatively insensitive to changes in the correction factors applied to the model. Concerning the difficulty in determining the rotor-casing heat transfer, it is reassuring to see that the influence of this correction factor (#1) is negligible.

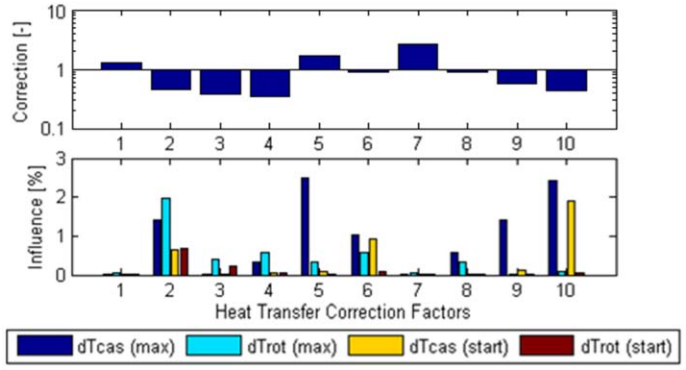

Figure 14: Correction factor magnitudes and sensitivity of the measured temperatures to a ±25% change.

5 TURBINE IMPROVEMENT MODIFICATIONS

Having established and validated a model allowing prediction of the temperatures within the steam turbine units, this can be then used to evaluate a number of proposed modifications to the turbine units which could potentially maintain the metal temperature during idle periods and thus reduce start-up time. In this study, three modifications are considered:

1. Installation of additional insulation material.
2. Installation of electrically-powered heat blankets, which provide heat to the external surface of the turbine casing underneath the insulation layer.
3. Increasing the temperature of the gland steam provided by the external supply during idle periods.

The impact of each modification on the casing and rotor of the turbine units will be quantified separately in order to examine the relative influence on both components. The results of applying the modifications to the steam turbines are shown in Figure 15. The values given for the casing and rotor improvement are the difference between the minimum temperature reached during cool-down with and without the measure applied.

5.1 Impact of Additional Insulation

The installation of additional insulation material would appear to have relatively little impact on the temperature of the casing of turbine, and no practical impact on that of the rotor

The low impact of additional insulation on the casing temperatures results from the fact that a significant thickness of insulation is already in place on both turbine units. As such, the heat loss to the environment from the casing through the insulation is already low, and reducing it further would require a doubling or tripling of the insulation thickness. Also, adding additional insulation does nothing to reduce heat losses to the bearings and condenser that begin to dominate the cool-down. In the case of the rotor temperatures, the negligible impact results from the very low rate of heat transfer across the flow passage. The small increase in casing temperature is therefore not effectively transmitted to the rotor.

5.2 Impact of Heat Blanket Installation

It can be seen in Figure 15 that the use of heat blankets is very effective in maintaining the temperature of turbine casing. However, this measure has a disappointingly low impact on the temperature of the rotor. This can be attributed to the low rate of heat exchange across the flow passage, resulting in the heat from the blankets being transferred almost exclusively to the turbine casing.

5.3 Impact of Gland Steam Temperature Increase

Increases in gland steam temperature affect both the casing and rotor of the steam turbine units. However, unlike the other two modifications analyzed, gland steam temperature has a greater influence on the rotor than on the casing. The relationship is practically linear in the range of temperatures studied.

The stronger impact of the gland steam temperature on the turbine rotors is due to the lower level of heat losses from the rotor. Unlike the casing which can lose heat through the insulation to the atmosphere, the rotor can only lose heat to the bearings and across the flow passage gap. As previously mentioned, heat transfer across the flow passage is limited. The effect of the bearing temperature on the central part of the rotor is limited by the fact that the bearing is located out beyond the labyrinth joints, which effectively shield the rotor from the influence of this temperature.

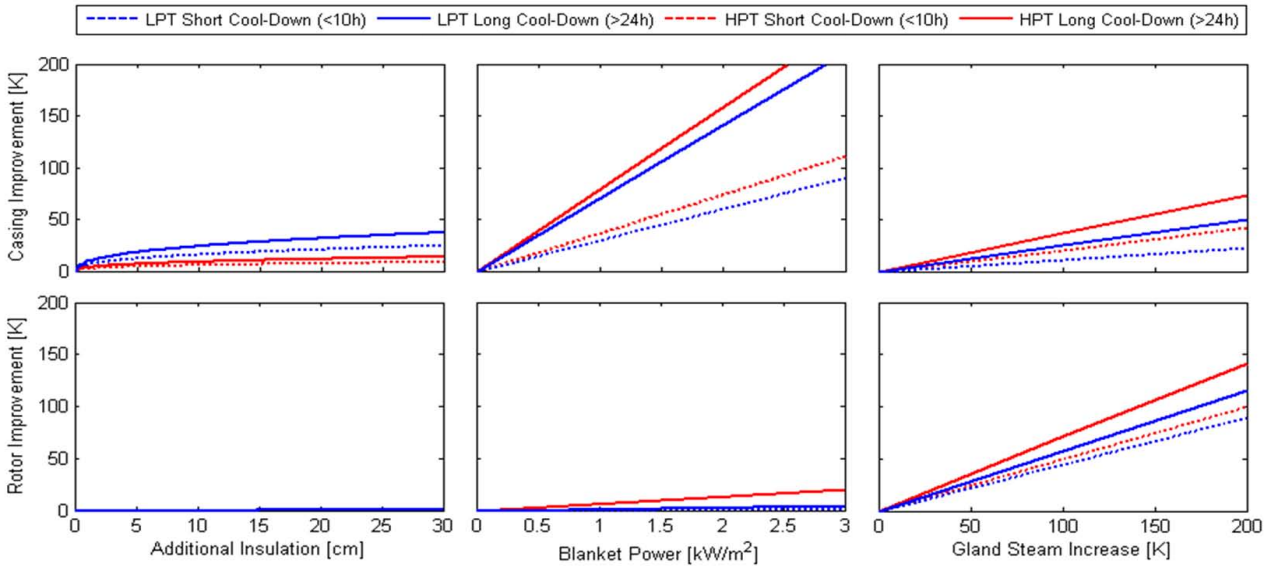

Figure 15: Impact of applying each of the three improvements to the steam turbine. Influence on the casing and rotor temperatures shown separately for both the high- and low-pressure turbines.

5.4 Suggestions for Turbine Improvement

The results in Figure 15 suggest that no single modification is sufficient to simultaneously create the necessary improvement in both the casing and rotor of the turbines that would allow faster turbine starts. Instead, it is proposed to combine the most effective modifications for each component, applying heat blankets to maintain the casing temperature, whilst increasing gland steam temperature in an effort to keep the rotor warm.

These results have also highlighted the importance of further work on determining the influence of the rotor temperatures. If only the casing temperatures had been studied, it could have been incorrectly concluded that applying heat blankets to the turbine units would have been sufficient to maintain the temperatures and permit moving to a faster start-up time.

6 PLANT PERFORMANCE IMPROVEMENT

In order to quantify the potential increase in power plant output that can be expected when applying the different modifications described above, it is necessary to take into consideration not only the extra electrical output resulting from faster start-up, but also the energy consumption of the heating measures. The increase in electrical output ΔE can be calculated using (10) where E_o is the nominal power of the steam turbine, Δt_{start} is the reduction in start-up time, Q_{blk} the power supplied to the heat blankets, M_{gst} the mass flow rate of gland steam when the turbine is idle, Δh_{gst} the increase in gland steam enthalpy and t_c the duration of the cool-down before start-up. In order to simplify analysis of the two different modifications, electrical heating of the gland steam is assumed.

$$\Delta E = \dot{E}_o^- \Delta t_{start} - \left(\dot{Q}_{blk} + \dot{M}_{gst} \Delta h_{gst}\right) \cdot t_c \qquad (10)$$

The reduction in start-up time when applying the different measures can be determined using the data in Figure 1, based on the minimum metal temperatures reached within both the turbine units before start-up begins.

As was suggested by the results in §5, it is necessary to apply a combination of two of the modifications in order to achieve a significant effect on the minimum cool-down temperatures. The two most effective measures, namely heat blankets and gland steam temperature increase, have been applied together in different intensities and the potential increase in turbine output determined. The results of this analysis are shown for long and short cool-down periods in Figures 16 and 17 respectively. Increase in daily output is given relative to a nominal day with 12 hours full-load operation of the solar power plant and the modifications are applied to both the high- and low-pressure turbine units.

The thinner, diagonal, contours in Figures 16 and 17 are lines of equal energy consumption for the turbine modifications, whereas the thicker contours represent a step change in daily electricity output resulting from moving to a faster start-up time.

Optimal points are highlighted in both figures, corresponding to points requiring minimum energy consumption to reach a given start-up time.

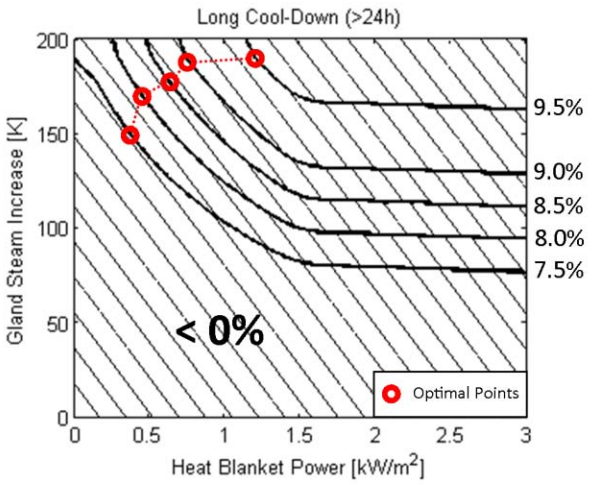

Figure 16: Increase in daily output resulting from the application of a combination of heat blankets and increased gland steam temperature on the day following a long cool-down period.

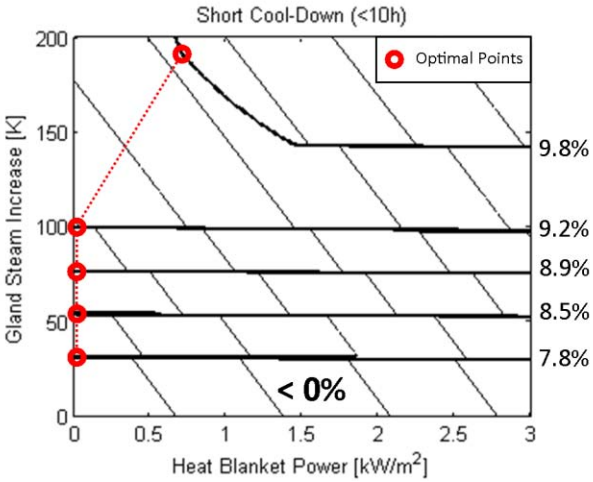

Figure 17: Increase in daily output resulting from the application of a combination of heat blankets and increased gland steam temperature on the day following a short cool-down period.

It can be seen that after a long cool-down, a strong increase in the gland steam temperature is necessary to reach even the lowest increase in daily production. Combining heat blankets with the increased gland steam temperature reduces the magnitude of heating required to achieve faster starts and can allow even faster start-up times to be achieved.

In the case of a short cool-down period, it possible to reach substantial increases in daily output with application of a gland steam temperature increase alone. Heat blankets become

necessary only in order to reach the higher start-up speeds (and thus daily productivity increases).

7 CONCLUSION

Transient behavior during steam turbine operation takes on a more important role in solar thermal power plants than in conventional base-load plants due to the increased frequency of turbine starts. This is especially true on days with sporadic insolation as the ability to start the plant rapidly allows the harnessing of solar resources that would otherwise be unavailable.

The dynamic steam turbine model presented in this study has shown itself to be a useful tool for analyzing the evolution of the turbine casing and rotor temperatures during transient operation. Validation against operation data from the Andasol 1 power plant has allowed confirmation that the key dynamics are well captured by the model. The study highlighted the fact that additional work is needed to examine the heat transfer between the casing and rotor of the turbine, with obtaining measurement data from within the rotor a key priority. Attempts are underway to examine the thermal expansion of the turbine rotor with a view to gaining insight into its temperature.

Of the three proposed modifications to the steam turbine units, additional insulation was shown to have little effect on the turbine metal temperatures during cool-down. Conversely, adding heat blankets was shown to have a significant impact on the temperatures in the casing and increased gland steam temperature had a strong influence on the temperatures in the rotor. The suggestion was made that combining these two modifications could be effective in maintaining the temperature of the turbine units; allowing faster turbine starts after idle periods. This was analyzed by evaluating the increase in daily electrical output of the power plant when different combinations of these measures were used. The results were very positive, showing potential increases in the range of 7-9%. It should be noted that these results are valid only for the two specific cool-down conditions presented in this study. A more complete study of the annual performance improvement is underway, considering a representative distribution of different cool-down times over the year.

Maintaining the temperature of the steam turbines during idle periods would seem therefore to be a viable possibility for solar thermal power plant operators. Doing so not only reduces the thermal stresses experienced by the units, extending their life-span, but also allows an increase in electrical output of the plant by making the turbines able to respond more quickly to the availability of solar insolation. Both these outcomes will serve to increase the economic viability of solar thermal power plants based on steam turbine technology, making them a more attractive alternative for investors, and thus accelerating the deployment of solar thermal power.

ACKNOWLEDGMENTS

The authors would like to thank the owners and operators of the Andasol 1 power plant for the opportunity to take on-site measurements of the steam turbine temperatures and their kind provision of the corresponding plant operation data.

Thanks are also given to the Industrial Energy Systems Laboratory of the Swiss Federal Institute of Technology, Lausanne for the use of their multi-objective optimization algorithm: QMOO.

This research has been funded by the Swedish Energy Agency, Siemens Industrial Turbomachinery AB, Volvo Aero Corporation, and the Royal Institute of Technology through the Swedish research program TURBOPOWER, the support of which is gratefully acknowledged.

REFERENCES

[1] Kosman G, Rusin A., *"The Influence of the Start-Ups and Cyclic Loads of Steam Turbines conducted according to European Standards on the Component's Life",* Energy, Volume 26 (2001), pp. 1083-1099

[2] Birnbaum J., Feldhoff J., Fichtner M. et al., *"Steam Temperature Stability in a Direct Steam Generation Solar Power Plant"*, SolarPACES Conference, Berlin, 2009

[3] Stuetzle T., Blair N., Mitchell J. et al., *"Automatic Control of a 30 MWe SEGS VI Parabolic Trough Plant"*, Solar Energy, Volume 76 (2004), pp. 187-193

[4] Emberger H., Schmid E., Gobrect E., *"Fast Cycling Capability for New Plants and Upgrade Opportunities"*, PowerGen Asia Conference, Singapore, 2005

[5] Birnbaum J., Jöcker M., Link K. et al., *"Simulation of the Dynamic Behaviour of Steam Turbines with Modelica"*, International Modelica Conference, Como, 2009

[6] Spelling J., Favrat D., Martin A. et al., *"Thermo-Economic Optimisation of Solar Tower Power Plants"*, International ECOS Conference, Lausanne, 2010

[7] Incropera F., De Witt D., *"Fundamentals of Heat and Mass Transfer"*, John Wiley & Sons, New York, 2007

[8] Quarteroni A., Saleri F., *"Scientific Computing with MATLAB, Second Edition",* Springer-Verlag, Berlin, 2006

[9] Eriksson K., Estep D., Hansbo P. et al. *"Computational Differential Equations",* Cambridge University Press, New York, 1996

[10] Cooke D., *"Modeling of Off-Design Turbine Pressures by Stodola's Ellipse"*, Energy Incorporated, Richmond, 1983

[11] Ray A., *"Dynamic Modelling of Power Plant Turbines for Controller Design"*, Applied Mathematical Modelling, Volume 4 (1980), pp. 109 – 113

[12] Leyland G, *"Multi-Objective Optimisation applied to Industrial Energy Problems"*, PhD Dissertation, Ecole Polytechnique Fédérale de Lausanne, 2002

[13] Marler R., Arora J., *"Survey of Multi-Objective Optimization Methods for Engineering"*, Structural and Multidisciplinary Optimization, Volume 26 (2004), pp. 369-395

